Online Resource 1 for:

Fullerton, A.H. C.E. Torgersen, J.J. Lawler, E.A. Steel, J.L. Ebersole, and S.Y. Lee. Longitudinal thermal heterogeneity in rivers and refugia for coldwater species: effects of scale and climate change. Aquatic Sciences

Table S1 Length of rivers surveyed with thermal infrared (TIR) remote sensing in each stream order class (TIR_{SO}) as a percentage of total length[a] of all rivers surveyed (TIR_{all}) and as a percentage of all reaches in the same stream order class (NHD_{SO}), and the length of reaches in a given stream order class as a percentage of the total length of all NHD reaches excluding first order streams (NHD_{all}). Weighted average stream order is 4.44 and 4.26 for reaches used by Pacific salmon and for all TIR reaches, respectively (and 2.99 for all NHD reaches)

Strahler stream order	TIR_{SO}/ TIR_{all} (%)	TIR_{SO}/NHD_{SO} (%)	NHD_{SO}/NHD_{all} (%)
2	8	1	50
3	18	3	25
4	22	8	12
5	24	15	7
6	18	24	4
7	4	13	0.1
7-9	1	8	<0.1

[a] TIR data were linked to reaches in the National Hydrography Dataset (NHD; nhd.usgs.gov) at a scale of 1:100,000

Table S2 Length of rivers surveyed with thermal infrared (TIR) remote sensing that are used by each species of Pacific salmon (TIR_{sp}) as a percentage of total length[a] of all rivers surveyed (TIR_{all}) and as a percentage of habitat[b,c] for the same species (Hab_{sp}), and the length of habitat for a given species as a percentage of the total length of all anadromous salmon habitat (Hab_{all})

Species	TIR_{sp} / TIR_{all} (%)	TIR_{sp} /Hab_{sp} (%)	Hab_{sp} /Hab_{all} (%)
Anadromous	72	15	100
Steelhead: summer	54	23	48
Steelhead: winter	34	10	68
Chinook: fall	22	19	25
Chinook: spring	47	33	29
Chinook: summer	8	27	6
Coho	33	13	34
Chum	4	9	9
Pink	2	13	4
Sockeye	8	27	6

[a] TIR data were linked to reaches in the National Hydrography Dataset (NHD; nhd.usgs.gov) at a scale of 1:100,000

[b] Pacific Northwest: www.streamnet.org/data/interactive-maps-and-gis-data (referenced to StreamNet's "best available mixed-scale routed hydrography" as of January 2012 (MSHv3) on the LLID-based stream routing system)

[c] California: www.calfish.org/ProgramsData/Species/AnadromousFishDistribution.aspx (steelhead and coho are 1:24,000 scale; Chinook data are 1:100,000 scale)

Table S3 Area of 10-digit watershed boundary dataset[a] units containing rivers surveyed thermal infrared (TIR) remote sensing containing each land use/land cover class[b] (TIR_{CL}) as a percentage of total area of all watersheds containing surveyed rivers (TIR_{all}) and as a percentage of area in a given class for all watersheds in the Pacific Northwest (USA), northern California and Great Basin (TIR_{CL}), and the area of watersheds in each class as a percentage of the total area of all watersheds in the region (WBD_{all})

Land use/land cover class (code)	TIR_{CL}/ TIR_{all} (%)	TIR_{CL}/WBD_{CL} (%)	WBD_{CL}/ WBD_{all} (%)
Evergreen forest (42)	44.7	6.8	25.5
Shrub/scrub (52)	25.3	2.3	41.4
Grassland/herbaceous (71)	7.7	3.7	8.1
Cultivated crops (82)	7.4	4.8	6.0
Pasture/hay (81)	3.6	7.4	1.9
Mixed forest (43)	2.6	7.5	1.4
Developed, open space (21)	2.2	5.2	1.7
Developed, low intensity (22)	1.3	5.7	0.9
Open water (11)	1.0	1.3	2.9
Emergent herbaceous wetlands (95)	1.0	7.1	0.5
Deciduous forest (41)	0.9	3.3	1.1
Barren land (rock/sand/clay) (31)	0.8	1.0	3.2
Woody wetlands (90)	0.7	6.2	0.4
Developed, medium intensity (23)	0.5	3.6	0.6
Developed, high intensity (24)	0.2	4.0	0.2
Perennial ice/snow (12)	<0.1	2.6	<0.1

[a] Watershed Boundary Dataset: http://nhd.usgs.gov/wbd.html

[b] Land use/land cover, 2011: http://www.mrlc.gov/nlcd2011.php

Table S4 Length of rivers surveyed with thermal infrared (TIR) remote sensing in each ecoregion (TIR_{ER}) as a percentage of total length[a] of all rivers surveyed (TIR_{all}) and as a percentage of all reaches in the same ecoregion[b] (NHD_{ER}), and the length of reaches in a given ecoregion as a percentage of the total length of all NHD reaches in Washington, Oregon, Idaho, and California (USA), excluding first order streams (NHD_{all})

Ecoregion (level and code)	TIR_{ER}/ TIR_{all} (%)	TIR_{ER}/NHD_{ER} (%)	NHD_{ER}/ NHD_{all} (%)
Level II			
Western Forested Mountains (6.2)	69.4	8.9	42.3
Coastal Forests (7.1)	18.2	10.4	9.5
Western Deserts (10.1)	11.4	2.8	21.9
Mediterranean California (11.1)	0.9	0.3	18.9
Other	0	0	7.4
Level III			
Blue Mountains (11)	21.1	16.9	6.8
Eastern Cascades Slopes and Foothills (9)	14.9	18.0	4.5
Klamath Mountains/California High North Coast Range (78)	11.4	13.2	4.7
Coast Range (1)	8.8	8.2	5.8
Columbia Plateau (10)	7.3	5.0	7.9
Willamette Valley (3)	6.7	16.8	2.2
Cascades (4)	6.4	7.5	4.6
Idaho Batholith (16)	5.6	5.9	5.2
North Cascades (77)	4.9	9.5	2.8
Northern Rockies (15)	3.5	3.8	5.0
Puget Lowland (2)	2.7	9.6	1.5
Northern Basin and Range (80)	2.5	1.5	8.7
Middle Rockies (17)	1.5	3.0	2.7
Central California Foothills and Coastal Mountains (6)	0.9	0.5	9.9
Snake River Plain (12)	0.7	1.0	3.6
Wyoming Basin (18)	0.6	15.7	0.2
Central Basin and Range (13)	0.4	1.2	1.6
Wasatch and Uinta Mountains (19)	0.2	6.0	0.2
Other	0	0	22.2

[a] TIR data were linked to reaches in the National Hydrography Dataset (NHD; nhd.usgs.gov) at a scale of 1:100,000
[b] Ecoregions: www.epa.gov/naaujydh/pages/ecoregions.htm. Omernik JM (1987) Ecoregions of the Conterminous United States Annals of the Association of American Geographers 77:118-125

Table S5 Distributions (quantiles) of conditions for each reach[a] surveyed with thermal infrared remote sensing

Percentile	Cumulative drainage area[b] (km^2)	Discharge[c] (m^2/s)	Velocity[d] (m/s)	Elevation[e] (m)	Slope[f] (%)	Max weekly summer air temperature[g] (°C)	Mean annual precipitation[h] (mm)	Probability of winter precipitation as snow[i]
0	0	0	0.3	0	0	10.0	156	0
5th	19	0.011	0.8	38	0	13.9	289	0.01
25th	181	0.088	1.2	268	0	16.2	449	0.01
50th	907	0.365	1.5	631	3e-3	17.7	645	0.65
75th	3,993	1.651	1.9	1,168	0.01	19.4	1,131	0.95
95th	20,500	6.844	2.8	1,678	0.03	21.7	2,134	0.97
100th	575,519	153.038	8.3	2,273	0.94	23.6	4,690	0.97

[a] TIR data were linked to reaches in the National Hydrography Dataset (NHD; nhd.usgs.gov) at a scale of 1:100,000

[b] TotDASqKM, PlusFlowlineVAA table, attributes of NHDPlusV2 (www.horizon-systems.com/nhdplus); McKay L, Bondelid T, Dewald T, Rea A, Moore R (2012) NHD Plus Verion 2: User Guide. Application-ready geospatial framework of U.S. surface-water data products associated with the USGS National Hydrography Dataset

[c] Q0001E, EROM model, attributes of NHDPlusV2

[d] V0001E, EROM model, attributes of NHDPlusV2

[e] Mean of MAXELEVSMO and MINELEVSMO, elevslope table, attributes of NHDPlusV2

[f] SLOPE, elevslope table, attributes of NHDPlusV2

[g] Mean of the maximum weekly air temperature, JA, 1970-1999; Wigmosta MS, Vail LW, Lettenmaier DP (1994) A distributed hydrology-vegetation model for complex terrain Wat Res Research 30:1665-1679

[h] V, IncrPrecipMA.txt, attributes of NHDPlusV2

[i] Climatic snow likelihood, DJF, 1979-2012 (zionklos.com/rain-snow_maps/); Klos PZ, Link TE, Abatzoglou JT (2014) Extent of the rain-snow transition zone in the western U.S. under historic and projected climate Geophysical Research Letters 41:4560-4568 doi:10.1002/

Table S6 Goodness of fit and residual trends for random forest models of longitudinal thermal profiles; percentiles were calculated from individual river profiles

	Percentile				
	2.5th	25th	50th	75th	97.5th
Model Goodness of Fit					
Mean Squared Error	0.011	0.038	0.109	0.273	1.228
Pseudo-R^2	0.592	0.886	0.970	0.989	0.997
Trends in Residuals[a]					
Intercept	-0.255	-0.071	-0.021	0.012	0.195
Slope	-0.014	-0.001	0.001	0.003	0.013
Adjusted R^2	-0.004	-0.002	0.001	0.006	0.057
Variable Importance Scores[b]					
Distance upstream	21.5	25.5	29.2	36.9	59.2
Summer air temperature	20.3	24.2	26.3	33.7	53.4
Mean annual precipitation	19.6	24.1	26.6	33.0	48.4
Winter snow probability	0	20.1	25.1	30.9	51.5

[a] Assessed by fitting linear models to the residuals of random forest models

[b] Ranging from 0 to 100

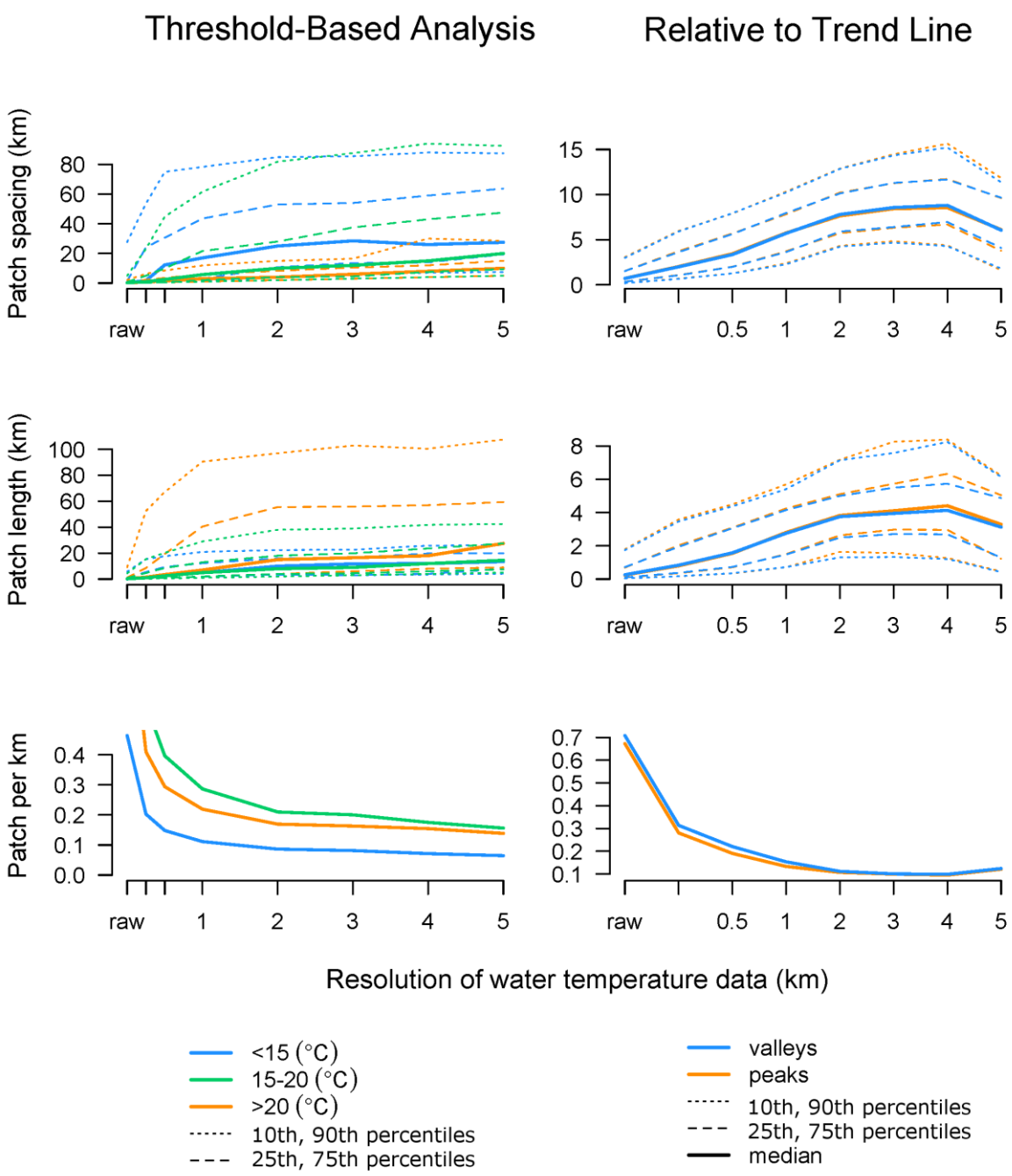

Fig. S1 Spacing, length, and density of patches quantified by partitioning longitudinal profiles into thermal zones (left panels) or as valleys or peaks from a moving average (right panels), as a function of the spatial resolution of the data. X-axis tick marks are labeled at resolutions we examined: raw is original thermal infrared survey data, and numeric values indicate data that were aggregated at 0.25-, 0.5-, 1-… and 5-km resolutions

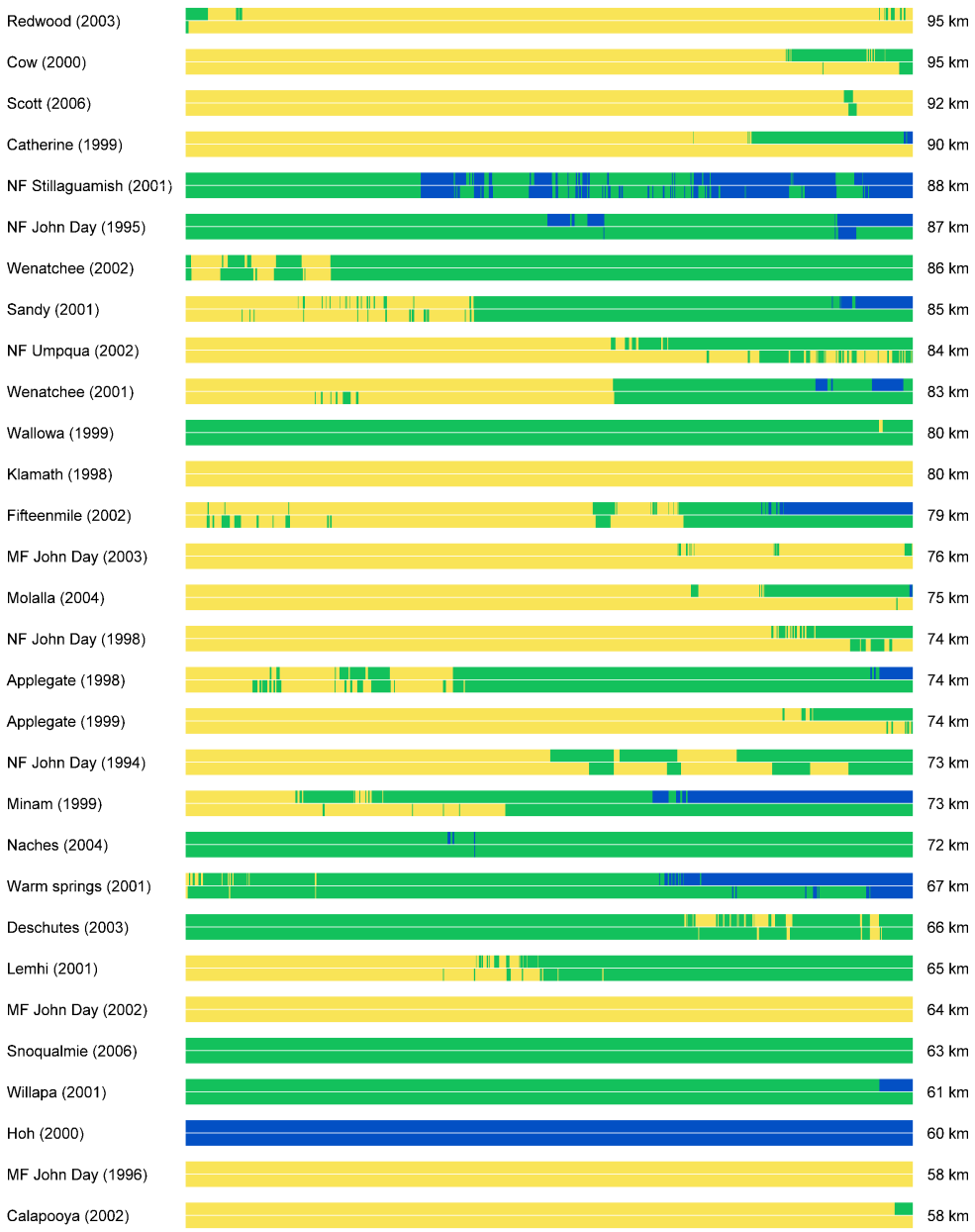

Fig. S2 Thermal heterogeneity in longitudinal profiles, depicted as proportional linear distance from the bottom of each survey (left) to the top of each survey (right). For each river, shading denotes patches >20 ˚C (yellow), 15-20 ˚C (green), and <15 ˚C (blue) based on analysis of thermal infrared (TIR) data surveyed in the year denoted parenthetically (top portion of each bar) and projected thermal heterogeneity for the 2080s based on random forest models (bottom portion of each bar). Plots illustrate patterns for the parts of the river accessible to anadromous fish; results for the surveys >95 km are shown in the main text

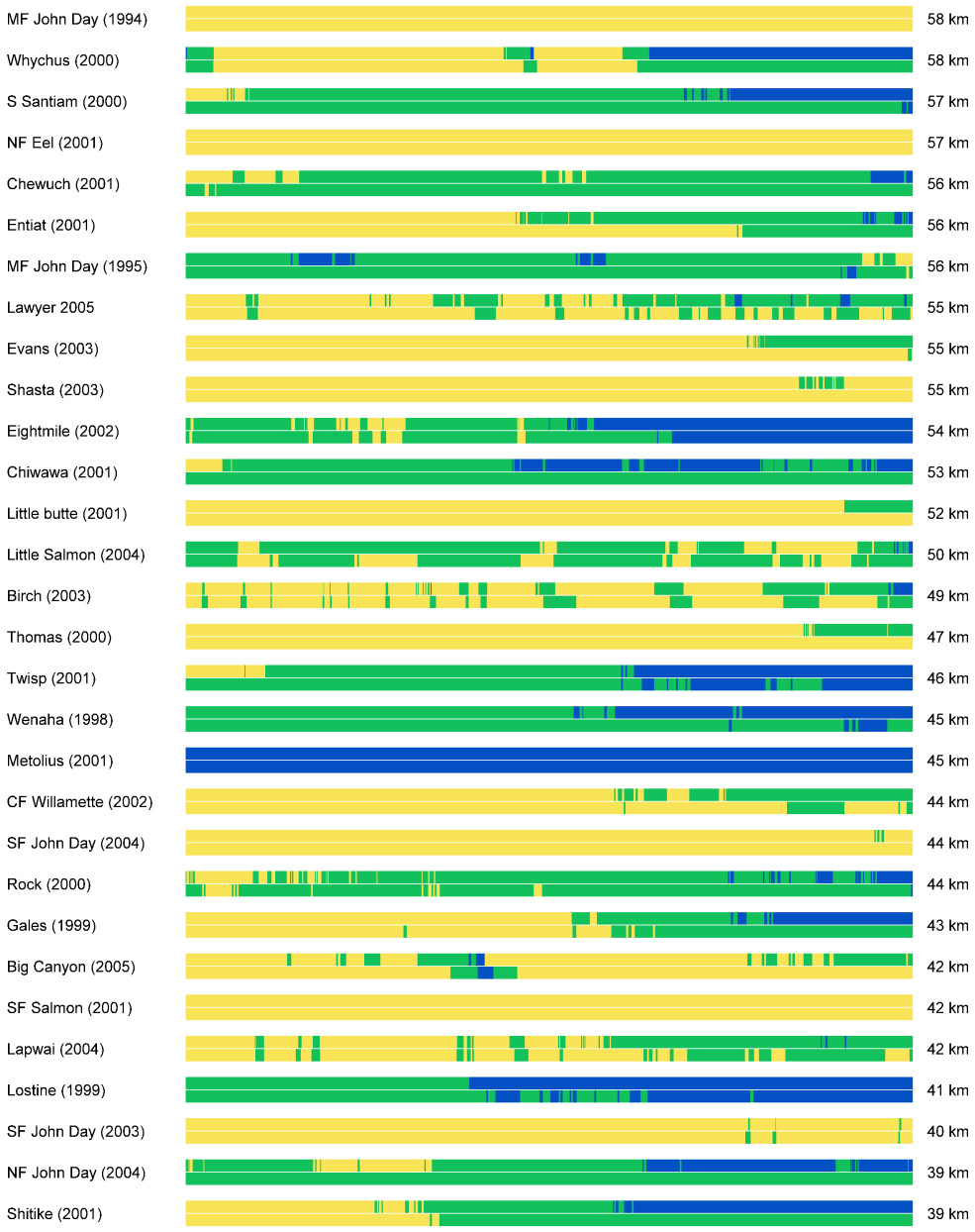

Fig. S2 Continued

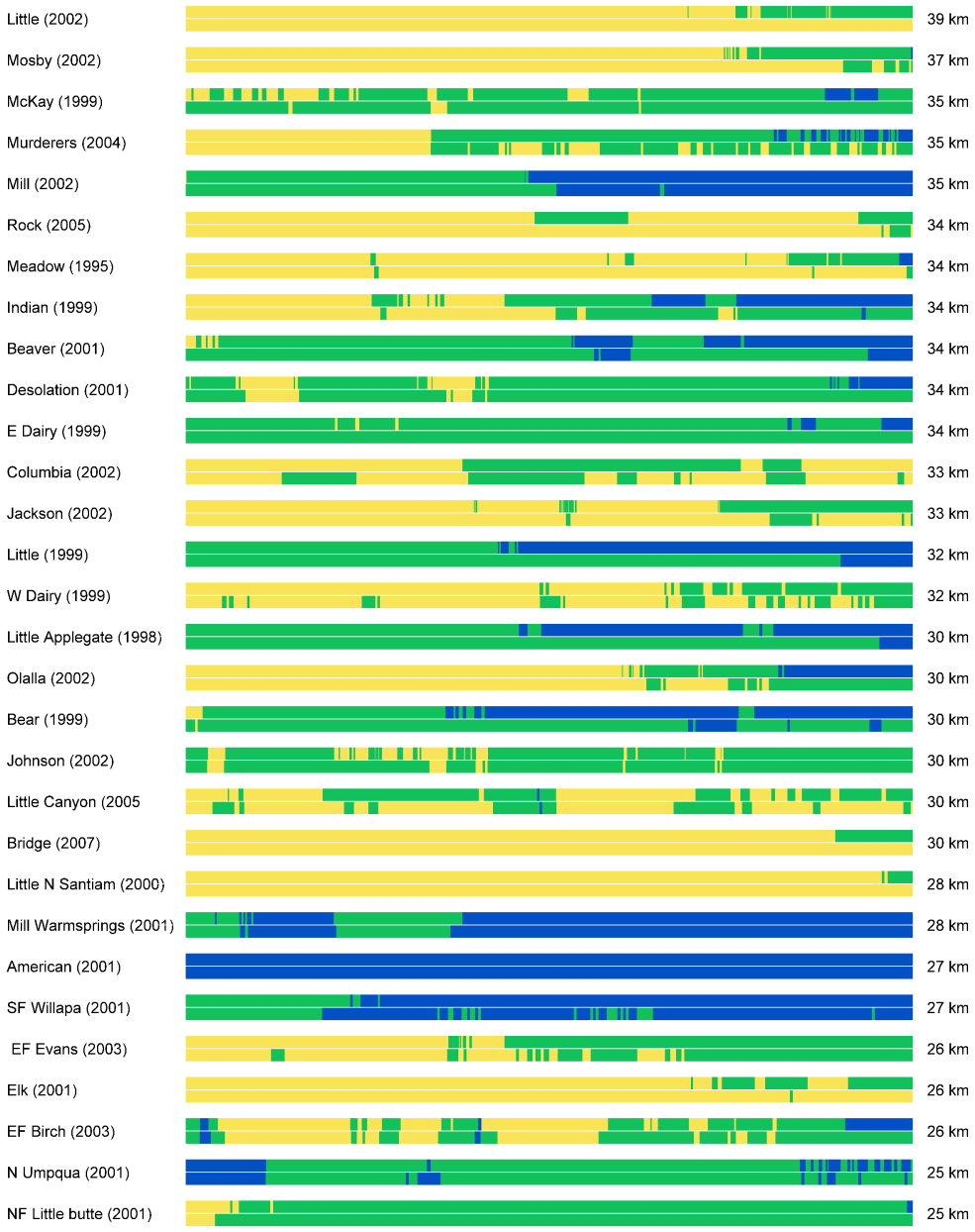

Fig. S2 Continued

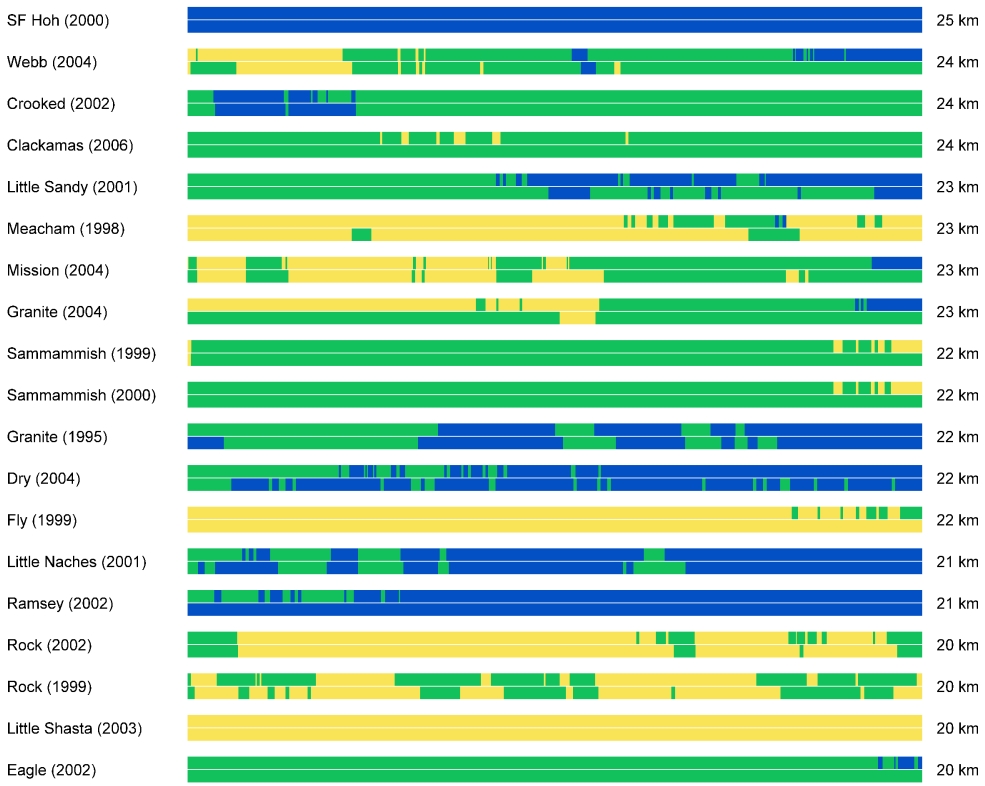

Fig. S2 Continued

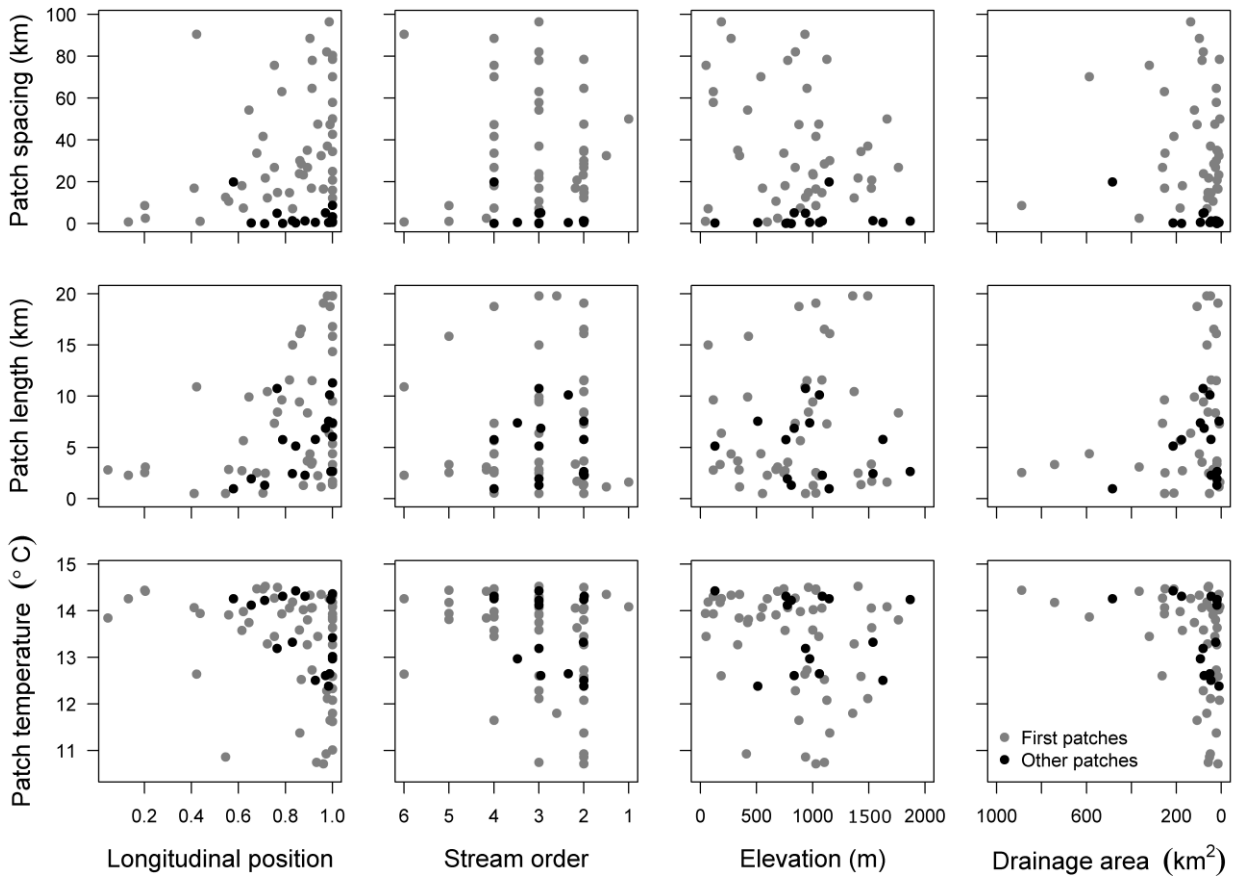

Fig. S3 Spacing, length, and mean temperature of cool thermal patches (<15 °C) in relation to proportional longitudinal survey position, Strahler stream order, elevation, and drainage area. The x-axes are arranged such that points on the left are downstream, higher in Strahler stream order, lower in elevation, and larger in drainage area. Plots display patches classified as likely to be important for Pacific salmon at an intermediate spatial scale (contiguous stretches >0.25 km and >2 °C cooler than adjacent water or >0.5 km and >1 °C cooler than adjacent water) for all rivers combined. The first patch encountered in each river (gray points) is differentiated from other patches located farther upstream (black points)

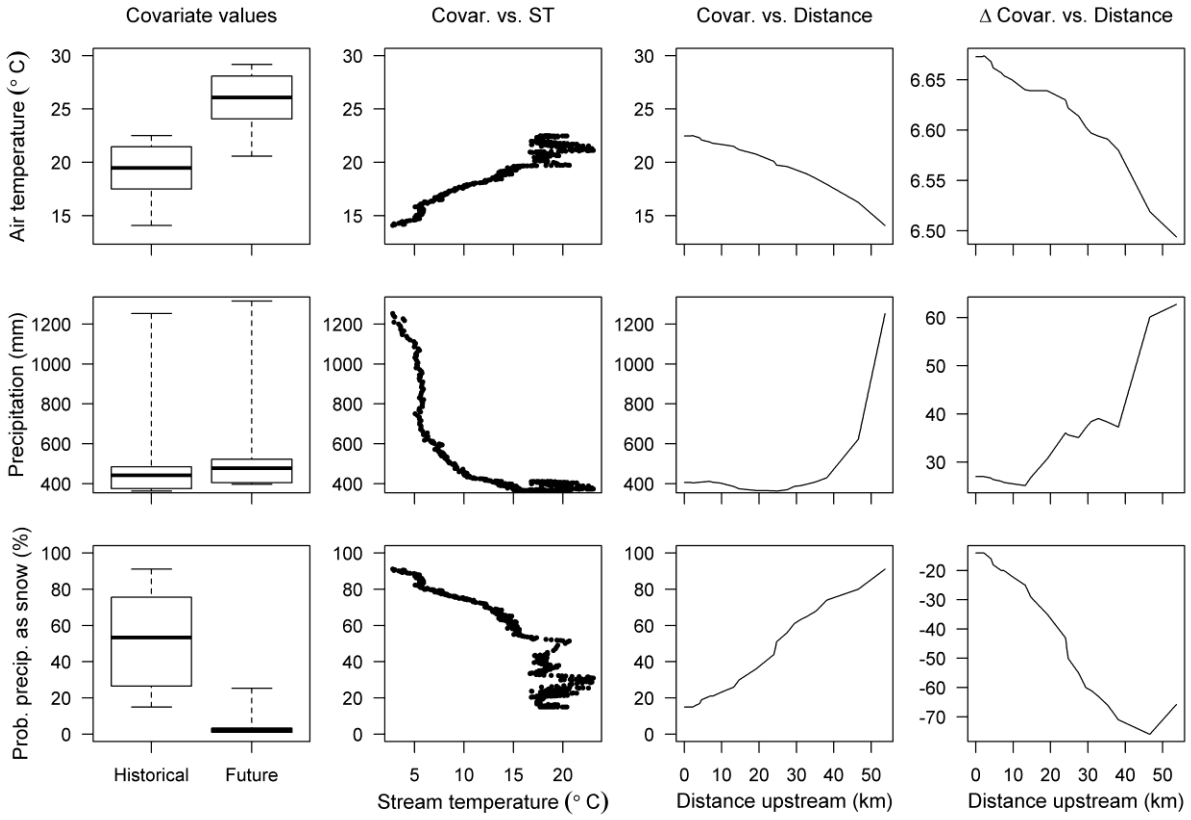

Fig. S4 Covariates used to fit past (1970-1999) and predict future (2070-2099) trends in water temperature (1st column), relationships between historical covariates and water temperature (2nd column), over the length of a river (3rd column), and expected change over the length of the river (4th column) for Eightmile Creek, a tributary to the Columbia River in Oregon, USA, surveyed on 3 August 2002. Variable importance scores were evenly distributed across covariates; mean prediction standard error would have increased by 24.8, 25.7, 25.0, and 25.2% if the model had not included distance upstream, air temperature, precipitation, or snow probability as covariates. The mean squared error and pseudo-R^2 for this model were 0.106 and 0.996, respectively

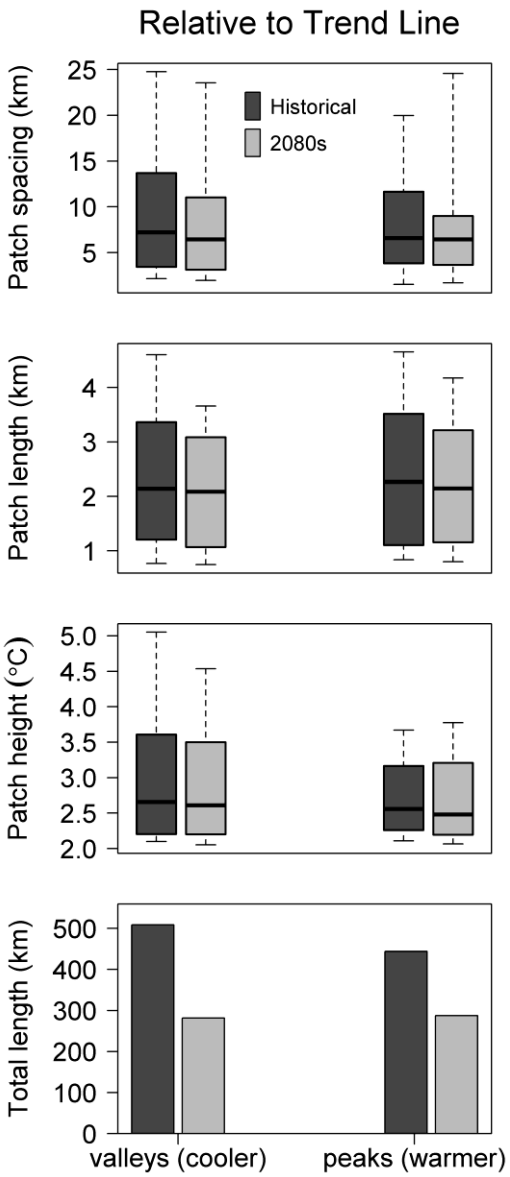

Fig. S5 Trend line-based summaries of valleys (cooler than the moving average) and peaks (warmer than the moving average), quantified for the raw thermal infrared survey data and for the 2080s climate scenario

Online Resource 2 for:

Fullerton, A.H. C.E. Torgersen, J.J. Lawler, E.A. Steel, J.L. Ebersole, and S.Y. Lee. Longitudinal thermal heterogeneity in rivers and refugia for coldwater species: effects of scale and climate change. Aquatic Sciences

Methods for Identifying Peaks and Valleys from a Moving Trend Line

We overlaid a smoothed trend on each longitudinal thermal profile (i.e., raw thermal infrared [TIR] data), and used the intersection of these lines to identify valleys (areas where TIR data fell below the trend line) and peaks (areas where TIR data exceeded the trend) that may be perceived as thermal refuges or barriers by fish. We computed the trend as a 10-km moving average so that results would be comparable across surveys of different length (other smoothing techniques are sensitive to length). We chose this level of smoothing to balance simplicity with the need to have a trend that was sinuous enough to reflect thermal heterogeneity at an intermediate spatial scale. Moving average computation shortens the length of a dataset (i.e., a centered 10-km moving average on a 50-km dataset yields a 40-km trend). To offset this loss of information, we duplicated the first and last 5 km of a dataset before smoothing to compute trends that extended to the full extent of the raw TIR data. We evaluated the effect of this decision by dividing long profiles into shorter segments and comparing the trends on these segments to the raw data; we found that differences between the raw data and the extended data were generally very small.

Projecting Future Water Temperature Patterns Using Climate Covariates

Methods – Using a geographic information system (GIS), we attributed each river reach in the National Hydrography Dataset, version 2 (McKay et al. 2012) with TIR temperature and a distance-weighted average of the nearest gridded values for three climate covariates suspected to be both highly related to water temperature and responsive to climate change: (1) maximum weekly air temperature between 16 July and 31 August, (2) mean annual precipitation, and (3) the proportion of precipitation that falls as snow during winter (December, January, February). Reaches were the spatial units used in statistical models.

We considered climate covariates from historical and future periods, where future values are representative of expectations under a greenhouse gas concentration scenario that is currently considered to be most likely: representative concentration pathway (RCP) 8.5, a high emissions scenario (Taylor et al. 2012). Data were derived from downscaled projections from the 10 General Circulation Models (GCM) described in the fifth phase of the Coupled Model Intercomparison Project (CMIP5) (Taylor et al. 2012). GCMs were statistically downscaled to $1/16^{th}$ degree resolution (about 5 x 7 km^2) for the western US using the Multivariate Adaptive Constructed Analogs (MACA) method (Abatzoglou and Brown 2012); we used the median of projections by the 10 GCMs. We computed gridded weekly maximum summer air temperature and mean annual precipitation data for the region; gridded data for the probability of winter precipitation falling as snow were obtained from Klos et al. (2014). The same historical (1970-1999; 1980s) and future (2070-2099; 2080s) periods were used for air temperature and precipitation; time periods for the probability of winter precipitation falling as snow differed slightly: 1979-2012 and 2035-2065. Estimates of this covariate are likely conservative for the 2080s.

We used random forest regression (Breiman 2001; Cutler et al. 2007) to construct relationships between water temperature the three climate covariates. We also included distance upstream (km) as a covariate. We chose random forest regression instead of other common techniques (e.g., generalized linear mixed-effects models or generalized least squares with correlated errors) because it is robust to anisotropy (data that are not stationary over space) and spatial autocorrelation (Cutler et al. 2007). Therefore, it accounts for spatial relationships between water temperature and covariates that differ over space. Moreover, data transformations are unnecessary, and this approach is good for making predictions (as compared to identifying causal relationships, which we were not assessing). Statistical analyses were performed in R using the randomForest package (Liaw and Wiener 2002).

For each river, we fit a random forest regression model between longitudinal thermal infrared stream temperature and co-located historical values of the climate covariates. We calculated a 10-km moving average trend for the fitted values to represent the portion of a longitudinal thermal profile's shape that was explained by the climate covariates. We extracted the residuals of a linear model between the raw stream temperature data and the trend. These residuals were interpreted as patchiness in longitudinal profiles that was not controlled by

climate covariates, but rather by controls on water temperature that we did not include in models, such as localized groundwater inputs, anomalies in adjacent landscape features or land use, network geometry or stream geomorphology. We then refit the model and trend for each river to predict future stream temperature by updating the climate covariates with values predicted for the 2080s. We added the residuals from the original fitted model to the future trend; these residuals represent variability that is unlikely to be influenced by changing climate conditions.

Results – Random forest models fit the data well (Table S6, Online Resource 1). For most rivers, mean squared error (MSE) values were well below 1, and pseudo-R^2 values exceeded 0.89 for three-quarters of rivers (all exceeded 0.59). There were no trends in residuals; intercepts, slopes, and adjusted R^2 values describing residuals were all near zero (Table S6). Across rivers, variable importance scores were evenly distributed among the four covariates. In decreasing order of importance, the contributions of the covariates were distance upstream, mean annual precipitation, summer air temperature, and winter snow probability (Table S6). Any given river may have been influenced more strongly by one covariate (e.g., air temperature) and not by another (e.g., snow probability).

References

Abatzoglou JT, Brown TJ (2012) A comparison of statistical downscaling methods suited for wildfire applications International Journal of Climatology 32:772-780 doi:10.1002/joc.2312

Breiman L (2001) Random forests Machine Learning 45:5-32

Cutler DR, Edwards TC, Jr., Beard KH, Cutler A, Hess KT, Gibson J, Lawler JJ (2007) Random forests for classification in ecology Ecology 88:2783-2792

Klos PZ, Link TE, Abatzoglou JT (2014) Extent of the rain-snow transition zone in the western U.S. under historic and projected climate Geophysical Research Letters 41:4560-4568 doi:10.1002/

Liaw A, Wiener M (2002) Classification and Regression by random Forest R News 2/3:18-22

McKay L, Bondelid T, Dewald T, Rea A, Moore R (2012) NHD Plus Verion 2: User Guide. Application-ready geospatial framework of U.S. surface-water data products associated with the USGS National Hydrography Dataset. URL www.horizon-systems.com/nhdplus/ (Jan 2014).

Taylor KE, Stouffer RJ, Meehl GA (2012) An Overview of CMIP5 and the Experiment Design Bulletin of the American Meteorological Society 93:485-498 doi:10.1175/bams-d-11-00094.1